Medial Axis Approximation with Constrained Centroidal Voronoi Diagrams On Discrete Data

Julien Dardenne, Sébastien Valette, Nicolas Siauve, Rémy Prost

CGI 2008 Conference Proceedings

Julien Dardenne · **Sébastien Valette** · **Nicolas Siauve** · **Rémy Prost**

Medial Axis Approximation with Constrained Centroidal Voronoi Diagrams On Discrete Data

Abstract In this paper, we present a novel method for medial axis approximation based on Constrained Centroidal Voronoi Diagram of discrete data (image, volume). The proposed approach is based on the shape boundary subsampling by a clustering approach which generates a Voronoi Diagram well suited for Medial Axis extraction. The resulting Voronoi Diagram is further filtered so as to capture the correct topology of the medial axis. The resulting medial axis appears largely invariant with respect to typical noise conditions in the discrete data. The method is tested on various synthetic as well as real images. We also show an application of the approximate medial axis to the sizing field for triangular and tetrahedral meshing.

Julien Dardenne · Sébastien Valette · Rémy Prost
CREATIS-LRMN, Université de Lyon, INSA, CNRS UMR 5220, Inserm U630 E-mail: name@creatis.insa-lyon.fr

Julien Dardenne · Nicolas Siauve
AMPERE, Université de Lyon, Université Lyon 1, CNRS UMR 5005
E-mail: nicolas.siauve@univ-lyon1.fr

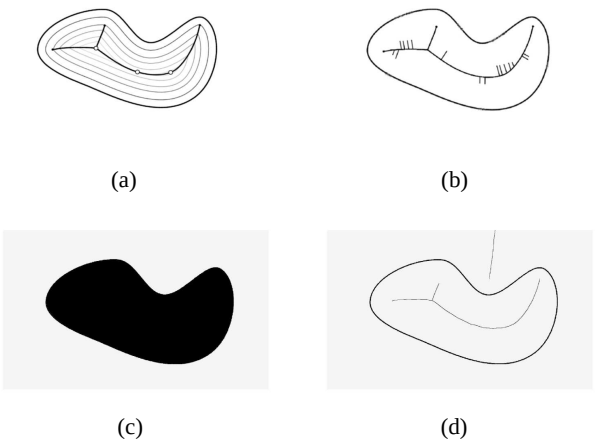

Fig. 1 A two-dimensional representation of the medial axis of a boundary *B* in the smooth and discrete case. Small perturbations on the boundary of the shape introduces larges ”spikes” in the medial axis.

Keywords Medial Axis · Discrete Data · Constrained Centroidal Voronoi Diagrams

1 Introduction

In the last forty years, the Medial Axis (MA) has been a constant research topic. The MA of a shape provides a compact representation of its features. The MA has been proposed as a tool for shape analysis, surface reconstruction, animation control, mesh generation and many other applications [1, 13, 14, 17]. A concise definition of the MA or skeleton in the smooth case was given by Blum [5], who postulated the well-known prairie fire (or grassfire) analogy [9]. The MA also can be defined as the set of centres of maximal balls which can fit inside a shape boundary. In figure 1 (a), we consider the MA of the shape in the smooth case. The fire front starts at the same time at every point on the boundary of a compact set *B*, moving with constant speed into *B*, locally perpendicular to the boundary and the place where two or more fronts collide defines the medial axis. In figure 1 (b), noise was added to the original shape and its skeleton was computed. One could see that the MA is very sensitive to noise and small pertubations on the boundary introduces large ”spikes” in the MA. The above definitions were formulated in smooth space. However, many of the applications that need MA approximation have discrete 3D datasets, such as those acquired using medical scanners. In discrete space, the definitions are analogous to the smooth case. In figure 1 (c), we proceed to the discrete case in adding to noise on the boundary shape. In the discrete case, with our approach the MA extraction is robust to noise (d) and the correct topology of the MA is found.

2 Contribution and Outline

This paper presents a discrete approach for approximate MA. This method is of completely discrete nature: it is especially designed for pixel or voxel data. It is based on a discrete definition of Constrained Centroidal Voronoi Diagram

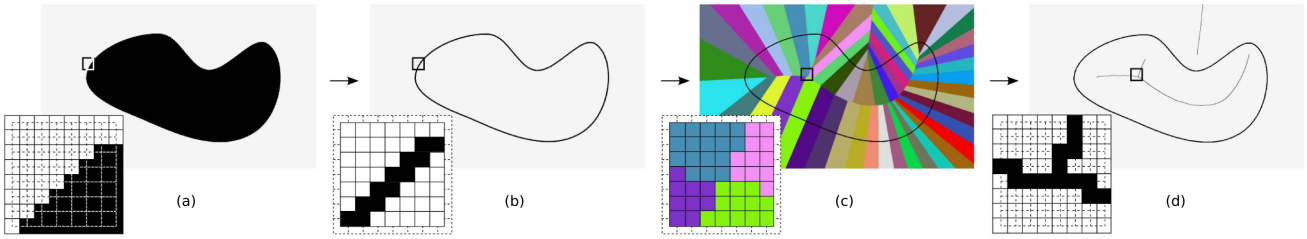

Fig. 2 From left to right : the shape in the primal graph (a); the shape boundary in the dual graph (b); its Constrained Centroidal Voronoi diagram (c); approximation of Medial Axis after filtering (d)

(CCVD) which provides an evenly distribued sampling of the shape boundary.

Figure 2 shows a summary of our approach. (a) shows the original shape. In (b), the boundary of the shape is detected. In (c), we construct the CCVD of the whole image, with the constraint that all the Voronoi sites lay on the shape boundary. The medial axis (d) is extracted from the VG by eliminating Voronoi edges intersecting the shape boundary and by filtering edges according to angle criterion.

The outline of this paper is as follows : In the next section, we review related works. Section 4 gives the preliminaries and definitions for this approach. In Section 5, we provide the details of the proposed approximation of MA definition and computation. In Section 6, we present the results of the algorithm and we compare our approach to others in the literature. Section 7 gives an exemple of application to mesh sizing function and we conclude in Section 8.

3 Related Works

In the following, we give a brief survey of approaches for MA extraction in the discrete or smooth case. This state of the art is far from being exhaustive due to the huge amount of existing methods. There are many approaches to compute the MA, but they can be broadly organised into three classes : distance transforms, thinning or morphological erosions and Voronoi approaches.

The distance functions, are based on the fact that the locus of the points of MA are coincidental with the singularities of a distance function to the boundary. A distance transform or distance field (D) is defined for each point x of a shape S as the smallest distance from that point to the boundary B_S of the shape:

$$D(x) = \min_{x \in B_S, y \in S} (d(x,y)) \tag{1}$$

where d is some distance metric. An appropriate distance metric (such as Euclidean or cityblock distance) is first used to calculate the distance transform of the shape. The local maxima of this distance function or the corresponding discontinuities in its derivatives are then detected, each of which indicates a point of MA [15]. In [8], Coeurjolly et al. present time optimal algorithms to extract the MA with the squared distance transform and the reverse Euclidean distance transformation. They explain the links between Euclidean Distance Transform and the construction of a VD.

Thinning, or morphological erosion, has been proposed to mimick Blum's grassfire formulation and operate by successively eroding points from the boundary of the object, while retaining the end points of line segments, until no more thinning is possible [24]. All thinning algorithms operate in the discrete space. They have been used on pixel and voxel image data in the areas of pattern recognition and image processing. Recently, an implementation of the fire front propagation in the discrete volume was proposed in [26].

There are also many approaches based on Voronoi Diagrams (VD) in the smooth setting [3].

Definition 1 Given an open set Ω of $\mathbb{R}^a$, and n different sites (or seeds) $z_{i;i=0,1,\ldots,n-1}$, the Voronoi Diagram (or Voronoi Tesselation) can be defined as n distinct cells (or regions) C_i such that:

$$C_i = \{w \in \Omega | d(w,z_i) < d(w,z_j)\, j = 1,2,\ldots,n, j \neq i\} \tag{2}$$

where d is a distance measure.

A survey of approaches for the construction of the medial axis (and Voronoi diagrams) is given by Sherbrooke et al. [12]. The MA is represented as a subset of the boundary of Voronoi cells defined within a compact set B by points on the boundary. The elements of MA are sets of points equidistant from at least two points on the boundary and their union represents a local symmetry axis of the shape. More specifically, it has been shown (for the 2D case in [6, 23] and for the 3D case in [11, 20]) that, under appropriately chosen smoothness conditions and as the sampling rate increases, the vertices of the VD of a set of boundary points will converge to the exact MA. In the smooth case, approximating the MA from the VD in 3D has been attempted in the past. The VD is deduced from the Delaunay Triangulation and then, a filtering is applied to the VD to approximate the MA. Dey and Zhao [11] compute the subset of the Voronoi facets or edges and vertices located inside the surface and then filter out some Voronoi vertices and their incident elements according to some angle and ratio criteria.

In medical image processing, real image data from computer tomography, magnetic resonance, with large amount

of voxels and noise, cause MA to be very dense and computation time to be expensive because they generate too many nodes and lines. There are two challenges to compute this approximation of MA :

– The MA is highly unstable with respect to small details of the shape.
– Only a discrete approximation of the MA is known and its sampling is dependent of the distribution of the input points.

4 Preliminaries and Definitions

Discrete shapes are defined to be a finite subset of the pixels or voxels of a space graph. The faces, edges, and vertices are collectively called boundary elements of the shape. For clarity reasons, we explain our approach in two dimensions. An image (or volume) is transformed into a graph such that, for each pixel (or each voxel) a vertex is associated, and pixels (or each voxel) that are neighbors in the sampling grid are joined by an edge [18]. This graph is denoted by $G = (V,E)$ and is called primal graph or neighborhood graph. Where V and E denote, the set of vertices, the set of edges, i.e. the set of unordered vertex pairs, respectively. The dual of this graph is the graph representing inter-pixel edges and inter-pixel vertices. This graph is denoted by $\overline{G}$ and is simply called dual graph.

The Discrete Voronoi Graph (DVG) is a graph of vertices and edges which are a subset of the CCVD. The vertices are the locus of points that have at least 3 pixels of different labels while the edges are the locus of points containing at least 2 pixels of different labels. In the discrete case, we call elements of the VG the boundary sub-edges incident to the pixels from the CCVD. There are a wide variety of edge detection algorithms in the literature, generally driven by neighbouring relationships.

We also can build a triangulation by dualizing the constructed diagram. There are a wide variety of algorithms available to build a Delaunay triangulation for a set of points in the smooth case. In fig. 3, an example of the relationship between Voronoi regions and Delaunay triangulation in two dimensions is given. The Voronoi sites Z_i are joined by a Delaunay edge if their Voronoi regions are adjacent. $E_{i,j}$ is an element of the DVG.

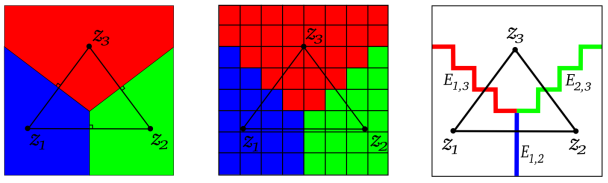

Fig. 3 Left: Delaunay Triangulation and its dual Voronoi Diagram in the smooth case; Middle: similar configuration in the discrete setting; Right: the DVG

5 Our Approach

This section describes the algorithm for constructing a MA approximation. Figure 4 provides an overview of this approach, consisting of three stages : the original model (a) is processed by our Constrained Centroidal Voronoi Diagram approach (b). The clusters anisotropy is measured by means of principal axis analysis (c). The DVG (d) is extracted from the CCVD following the neighbouring relationship. Finally, an approximation of the MA is created (f) by filtering the Voronoi element sets of the DVG (e).

5.1 Clustering algorithm

Our proposal is to construct the VD by a constrained clustering, where each cluster boundary potentialy represents a subset of the MA. The performance of the MA approximation approaches is usually dramatically reduced if the input shape is noisy. To address this problem, we propose to filter by clustering and then subsample the boundary B of the shape, while constructing the VD in the image.

5.1.1 Centroidal Voronoi Diagram

In this subsection, we make an overview of Centroidal Voronoi Diagrams (CVDs). The work presented here is closely related to the work of Valette et al. [25].

A CVD is a Voronoi diagram where each Voronoi site z_i is also the mass centroid of its Voronoi region :

$$z_i = \frac{\int_{C_i} x.\rho(x)dx}{\int_{C_i} \rho(x)dx} \tag{3}$$

where $\rho(x)$ is a density function. CVD minimize the energy given as:

$$E = \sum_{i=1}^{n} \int_{C_i} \rho(x)\|x - z_i\|^2 dx \tag{4}$$

Practically, a centroidal distribution of points is useful because the points are well-spaced. CVDs optimize the compactness of the created Voronoi regions and can be done, using algorithms such as k-means or Lloyd relaxations.

5.1.2 Constrained Centroidal Voronoi Diagram

We want to construct a CVD on a discrete input. Our approach is based on partitioning (clustering) the discrete input in a variational framework, which groups discrete cells into K clusters through the minimization of the total intra-cluster variance. Our algorithm is based on the construction of a partitioning which minimizes equation (4). It is possible to efficiently minimize with an iterative algorithm that updates the clustering according to tests on the boundaries between the different clusters. Here, we choose $\rho(x)$ to be uniform. The shape boundary is used for initial clustering.

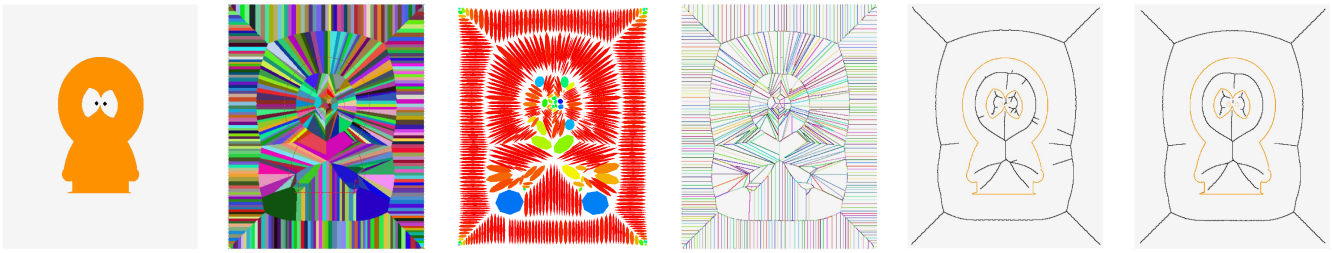

(a) (b) (c) (d) (e) (f)

Fig. 4 The original model (a) is processed by our Constrained Centroidal Voronoi Diagram approach (b). The clusters anisotropy is measured by means of principal components analysis (c). The DVG (d) is extracted from the CCVD following the neighbouring relationship. Finally, an approximation of MA is created by filtering the Voronoi element sets of the DVG (e and f).

Then, we define the digital shape as the set of all vertices labelled as boundary or not boundary. At each cluster C_i is associated a site. The major difference with [25] is that the site is defined as the center of mass of only the boundary vertices contained in the cluster. We also add an additional constraint to our clustering algorithm : to ensure diagram conformity, a cluster must always contain at least one boundary vertex.

We assume that the subsampling factor of this clustering is high, i.e the ratio between the number of original boundary vertices and the number of sites of the VD is high. We then have to evaluate of the optimal number of clusters. If we have few clusters, it is difficult to define the shape of the object. In the opposite case, using many clusters, "spikes" appears on the medial axis. Figure 4 shows an example of constrained clustering on a shape with 400 clusters.

We now define the various graphs extracted from the CVD. The motivation behind this dualisation is a good approximation of the boundary Voronoi cells for a better localization of the MA of the discrete shape. During the next step of the method, the constructed CCVD should be transformed into a DVG and the Delaunay Triangulation can be computed.

5.2 Filtering conditions

In this subsection, we describe the filtering algorithm. It is well-known that the MA is very sensitive to small perturbation of the shape boundary and many filtering methods have been proposed to remove bad components associated with noise or other artifacts. [7, 16] and [10] give a state of art of these approaches in the smooth case. Our aim is to approximate the MA with a subset of Voronoi edges or facets. i.e to decide if a given vertex set belongs or not to the MA. Our algorithm uses two criteria to select the Voronoi elements from the DVG.

5.2.1 Mesuring clusters anisotropy and principal axes

Following the general observation that the Voronoi cells are elongated along the normal direction at the boundary points [2], our algorithm measures the anisotropy of each cluster C_i in order to have a confidence measure on the normal estimation. For each C_i, we compute its covariance matrix M_i and deduce the local cluster anisotropy from the eigenvalues of M_i [22]. M_i can be viewed as a 3 x 3 tensor. The eigenvalues and eigenvectors of this symmetric and positive definite matrix correspond to the axes lengths and directions of an ellipsoid, respectively. We can deduce the principal axis from the eigenvector associated to the highest eigenvalue of M_i. The fractional anisotropy (FA_i) allows to compute the local anisotropy of each C_i [4] :

$$FA_i = \frac{\sqrt{3}}{\sqrt{2}} \frac{\sqrt{(\Lambda_i^1 - \overline{\Lambda_i})^2 + (\Lambda_i^2 - \overline{\Lambda_i})^2 + (\Lambda_i^3 - \overline{\Lambda_i})^2}}{\sqrt{(\Lambda_i^{1^2} + \Lambda_i^{2^2} + \Lambda_i^{3^2})}} \tag{5}$$

with :

$$\overline{\Lambda_i} = \frac{(\Lambda_i^1 + \Lambda_i^2 + \Lambda_i^3)}{3} \tag{6}$$

where $\Lambda_i^{j,\, j=1,2,3}$ are the eigenvalues of M_i, with $\Lambda_i^1 > \Lambda_i^2 > \Lambda_i^3$.

One note that :

$$0 \leq FA_i \leq 1 \tag{7}$$

The FA_i index is zero in a perfect isotropic case (a sphere) and 1 in the anisotropic case (the hypothetical case

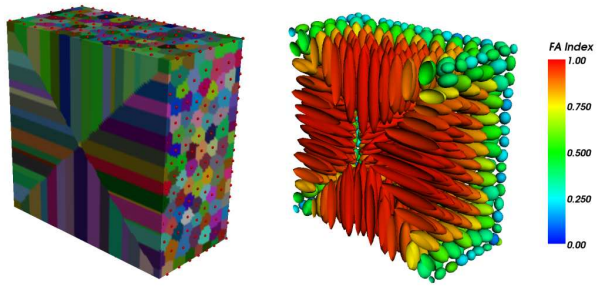

Fig. 5 Left: a cut of the Constrained Centroidal Voronoi Diagram of emty box with 1000 Voronoi cells. Right: each cluster is replaced by its equivalent ellipsoid. The FA_i shows the local anisotropy of each cluster C_i.

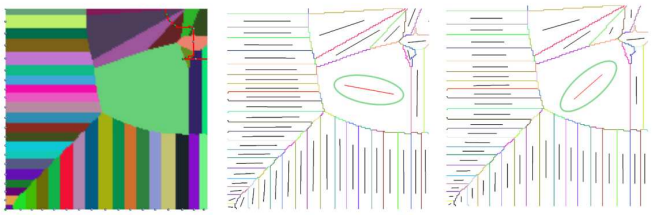

Fig. 6 Left: Centroidal Voronoi Diagram of the portion of the figure 4. Middle : estimation of principal axis for each cluster. Right: after correction, the encircled direction is now correctly estimated.

of an infinite cylinder). Increasing FA_i values indicate a higher tensor anisotropy. Figure 5 (left) shows a cut-view of the CCVD of an empty box (for wich the cube boundary defines the shape boundary). In figure 5 (right), each cluster is replaced by its equivalent ellipsoid. The ellipsoids elongation clearly depict the cluster anisotropy.

Sometimes, a cluster is mostly isotropic (i.e FA_i is close to 0) and its first principal axis does not approximate the normal direction. We detect these cases with the following test :

$$d(\overline{C_i}, z_i) > \alpha \,.\, \Lambda_i^1 \tag{8}$$

where Λ_i^1 is the principal eigenvalue of C_i, $\overline{C_i}$ is its barycenter and α is a arbitrary constant (in our experiments, we set $\alpha = 0.6$). Whenever this test is true for a cluster, we estimate its normal direction as :

$$\overrightarrow{N_i} = \frac{\overrightarrow{\overline{C_i} z_i}}{\|\overrightarrow{\overline{C_i} z_i}\|} \tag{9}$$

In figure 6 (middle), the principal axis (encircled) gives a bad approximation of the normal direction. Then, we compute the normal direction as above and obtain a good approximation of the normal direction (right).

5.2.2 Pole condition

Amenta et al. were the first to propose the definition of poles [19] and proposed the Powercrust algorithm [20] to construct manifold triangulations of three-dimensional points. When the boundary B is sufficiently dense, the Powercrust is guaranteed to produce a geometrically and topologically correct approximation. We recall that the set of poles is a subset of Voronoi vertices. In 2D, all Voronoi vertices converge to the medial axis. In 3D, some Voronoi vertices may be far from the medial axis but poles are guaranteed to converge to the medial axis. Each boundary-point is associated with two poles, denoted by p_{i+} and p_{i-}, respectively. These two poles are the farthest Voronoi vertices of Voronoi cell. The boundary B also is divided in two sets of poles: inside and outside poles. The definition of poles plays an important role in normals approximation. When B is a sufficiently densely sampled, the Voronoi cells appear naturally anisotropic, and are approximately perpendicular to the boundary of the shape. Our approach is based on an estimate of the vertices position with respect to the shape boundary and the estimated normal direction. We define the discrete element $E_{i,j}$ as the set of vertices adjacent to the clusters C_i and C_j. The critical part consists in tagging each vertex of each element as *positive* or *negative*. For each element $E_{i,j}$, we define an operator $f_{(i,j)}$ as follows:

$$f(i,j) = \begin{cases} i \text{ when } FA_i > FA_j \\ j \text{ when } FA_j > FA_i \end{cases} \tag{10}$$

We denote its site as $z_{f(i,j)}$ and its estimated principal axis $N_{f(i,j)}$. This allows a good approximation of the normal direction $N_{f(i,j)}$ to the shape boundary.

In this regard, a vertex candidate $v \in E_{i,j}$ will be tagged as negative or positive depending on the sign of $S_{f(i,j)}(v)$ defined as :

$$S_{f(i,j)}(v) = < \overrightarrow{z_{f(i,j)} v}, \overrightarrow{N_{f(i,j)}} > \tag{11}$$

$S_{f(i,j)}(v)$ then provides an information on v with respect to the boundary shape. We then define the first filtering condition as follows :

$$E_{i,j} \in MA \; if \; S_{f(i,j)}(v_1).S_{f(i,j)}(v_2) \geq 0, \quad \forall (v_1, v_2) \in (E_{i,j} \otimes E_{i,j}) \tag{12}$$

If an element $E_{i,j}$ contains vertices v for which $S_{f(i,j)}(v)$ is not always of the same sign, it can be deduced that this element crosses the shape boundary, and therefore is not considered as MA element. In the opposite case, all elements with the same sign belongs to the same side of the boundary. However, we do not know if they are inside or outside of the shape. Figure 7 shows two examples where $E_{1,2}$ is rejected for inclusion in the MA, and $E_{1,3}$ is considered as a part of the MA.

Our objective is to extract a simplified MA. However, in some cases, we see some "spikes" appearing on the MA. Then we use an angle condition to filter out some spikes at the poles condition.

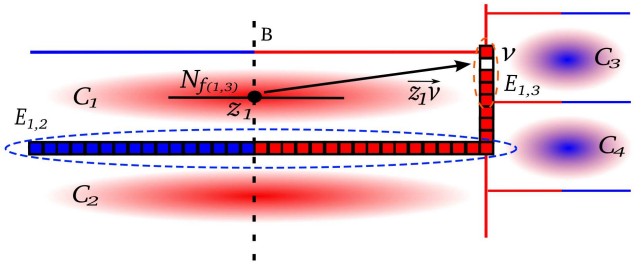

Fig. 7 A candidate vertex $v \in E_{1,3}$; $E_{1,3}$ does not cross the shape boundary as its vertices are all tagged same way; $E_{1,2}$ crosses the shape boundary as its vertices are not always tagged wich the same sign. As a consequence $E_{1,3} \in MA$ and $E_{1,2} \notin MA$;

5.2.3 Angle condition

An angle condition can be used to remove points from straight edges to eliminate spikes in the MA. Dey and Zhao [11] use a criteria on a angle condition to retain faces from the VD of a set of boudary points. They consider the angle between an approximate of the normal direction at the boundary points and a Delaunay edge (dual to a Voronoi face). If that angle is small, the Voronoi face is kept as a part of the MA.

Our method is based on the direct construction of the VG in the discrete space. Therefore, we consider the angle between the normal of an element of the VG (dual to a Delaunay edge) and the normal direction at the shape boundary wich is estimated by the principal axis associated with each surrounding cluster. For each boundary element candidate $E_{i,j}$, we associate an angle $\Theta_{i,j}$.

$$\Theta_{i,j} = \angle N_{f(i,j)}, N_{i,j} \tag{13}$$

The approximation of the angle $\Theta_{i,j}$ for a MA element requires both the knowledge of the principal axis $N_f(i,j)$ of the neighbouring cluster having the greatest anisotropy and the estimated normal direction of $E_{i,j}$, noted $N_{i,j}$. The scalar product is useful when you need to calculate the angle between two vectors. Then, we define the angle filtering condition as :

$$E_{i,j} \in MA \; if \; A_{i,j} > \gamma, \; \Lambda^1_{f(i,j)} > \beta \; . \; \Lambda^3_{i,j} \tag{14}$$

with

$$A_{i,j} = | < N_{f(i,j)}, N_{i,j} > | \tag{15}$$

where $\Lambda^1_{f(i,j)}$ and $\Lambda^3_{i,j}$ are the largest eigenvalue of $C_{f(i,j)}$ and the minimal eigenvalue of $E_{i,j}$, respectively, and γ and β are arbitrary. (in our experiments, we set $\gamma = 0.8$ and $\beta = 0.7$) Figure 8 shows an illustative example where $A_{i,j}$ is computed.

6 Results

The proposed algorithms has been tested with several discrete data. These algorithms were implemented in C++ using the VTK library.

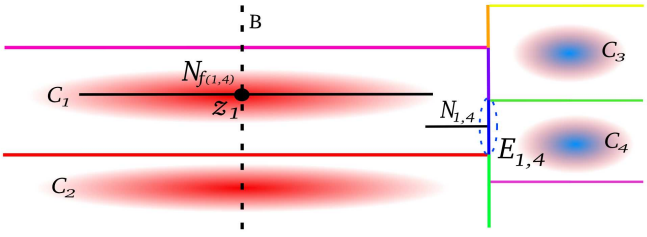

Fig. 8 The angle condition : the angle between $N_{f(1,4)}$ and $N_{1,4}$ has to be within a given range, or the element $E_{1,4}$ will be filtered out from the MA.

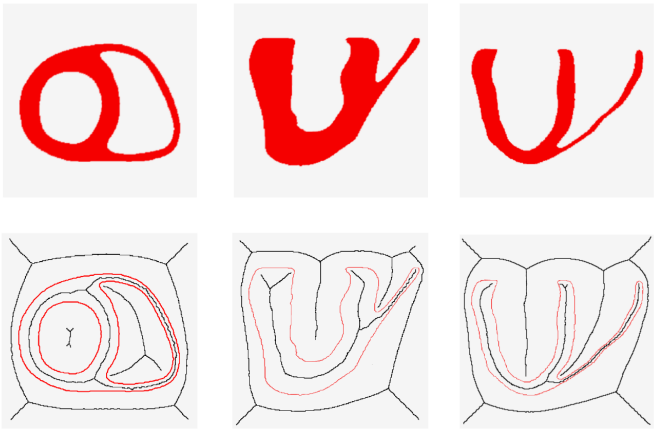

Fig. 9 Three slices of a volume representing a heart and their respective Medial Axis

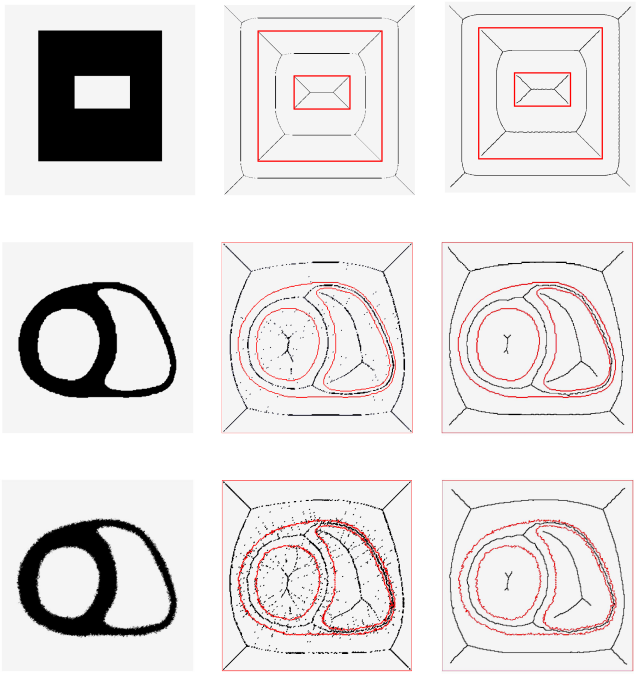

Fig. 10 Comparison between our approach and the RDMA approach [8]. Left : original shape. Middle : RDMA; Right : our approach

Figure 9 shows the results obtained on three different slices of a volume representing a human heart.

Figure 10 shows comparative results between our approach and the RDMA approach [8]. The first column is the original shape. The second column are the results obtained with RDMA. The third column was obtained with our approach. The first row shows a simple shape with sharp corners. The second row shows a slice of a human heart. The third row shows the same human heart but with noise on the shape boundaries. One can clearly see that in our approach the MA is smooth and connex for the three cases.

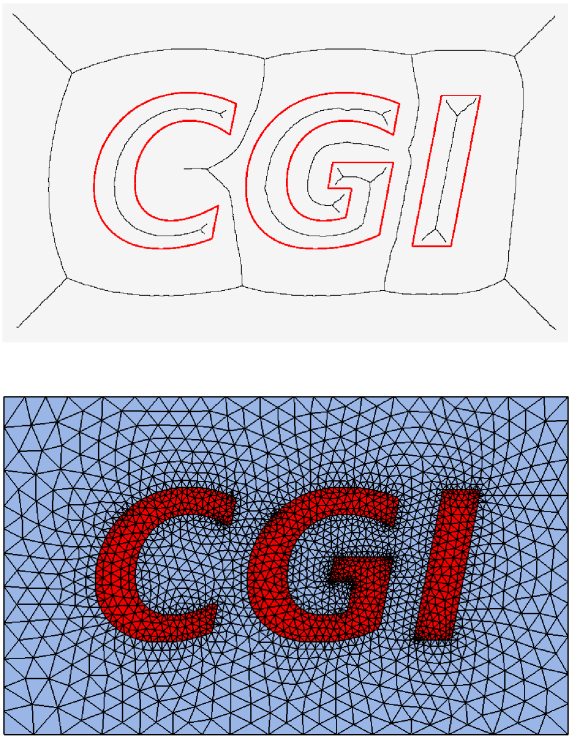

Fig. 11 On the top, approximation of the Medial Axis. On the bottom, 2D Delaunay triangulation with 2000 vertices.

7 Application to sizing function for mesh generation

Mesh sizing is one important aspect of the mesh generation problem.The size of the elements may be either a consequence of the meshing algorithm when no sizing constraints are provided as input, or may be explicitly controlled by the user or by the physical simulation carried on over the mesh. Several techniques have been proposed for automatic generations of mesh size function. Quadros and al. [26] used medial axis generation over domain boundaries to construct mesh sizing functions. For our experimentations, we used the definition of Alliez et al. [21] who proposed a sizing function $\mu(x)$ which provides the element size at each point x. Figures 11 and 12 show MA approximations of the letters "CGI" and a "bird" shape. One can see the influence of the MA then mesh sizing, as meshing density is higher in thin regions (the bird nozzle and tail regions).

Figure 13 shows a similar process for the 3D volume containing a human heart.

Our experiments support that both angle and dual conditions together produce a good approximation to the actual MA. Furthermore, the algorithm showed strong resistance against noise and boundary distorsion.

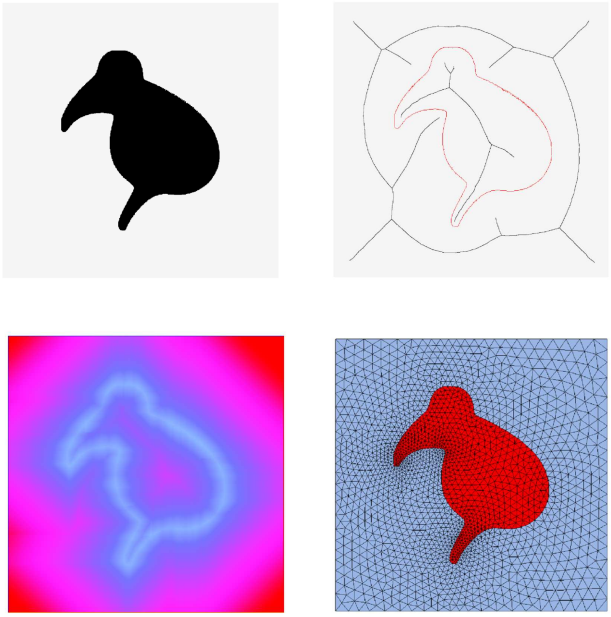

Fig. 12 Top : a shape (left) and its medial axis (right). Bottom : On the left, sizing function on the MA in 3D. The colors represent the sizing values. On the right, mesh generated with respect to the sizing function.

8 Conclusions

In this paper, we have presented an approach that approximates the medial axis for pixel or voxel objects. This approach is based on the Voronoi graph computed from a set of nodes distributed across the boundary. One of the key aspects is its completely discrete nature. Experimental results have shown that the method creates Medial Axis approximations which are robust to noise, and very suitable for mesh generation. Future work may include robust filtering of the MA elements, in order to increase the robustness of the approach.

Acknowledgements The Human heart data are courtsey of Dr Patrick Clarysse from CREATIS at Lyon. This work was supported in part by the BioRFMod project (ANR-06-JCJC-0124-01) and the Région Rhône Alpes Cluster 2 ISLE, PP3, subproject I3M: Imagerie Médicale et Modélisation Multiéchelles : du petit animal à l'Homme.

References

1. A. Bonnassie, F. Peyrin and D.Attali: Shape description of three-dimensional images based on medial axis. In: Proceedings. 2001 International Conference on Volume 3, pp. 931–934 (2001)
2. Amenta, N., Bern, M.: Surface reconstruction by voronoi filtering. In: SCG '98: Proceedings of the fourteenth annual symposium on Computational geometry, pp. 39–48 (1998)
3. B. Miklos, J.G., Pauly, M.: Medial axis approximation from inner voronoi balls: a demo of the mesecina tool. In: SCG '07: Proceedings of the twenty-third annual symposium on Computational geometry, pp. 123–124 (2007)

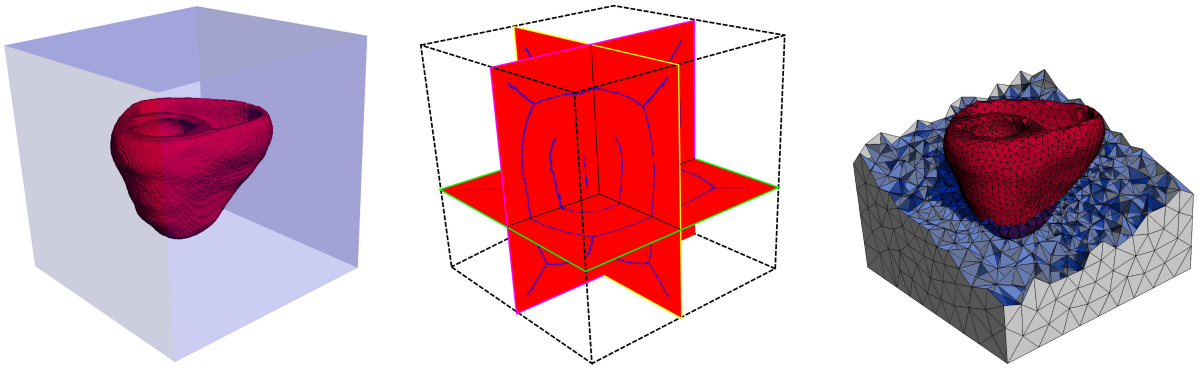

Fig. 13 Left : a volume representing a human heart. Middle : its Medial Axis. Right: mesh generated with respect to the sizing function (10000 vertices).

4. Basser, P.J., Pierpaoli, C.: Microstructural and physiological features of tissues elucidated by quantitative-diffusion-tensor mri. Journal of Magnetic Resonance pp. 209–219 (1996)
5. Blum, H.: A transformation for extracting new descriptors of form. Models for the Perception of Speech and Visual Form pp. 362–380 (1967)
6. Brandt, J.W., Algazi, V.R.: Continuous skeleton computation by voronoi diagram. CVGIP: Image Underst. **55**(3), 329–338 (1992)
7. Chazal, F., Lieutier, A.: The lambda medial-axis. Graph. Models **67**(4), 304–331 (2005)
8. Coeurjolly, D., Montanvert, A.: Optimal separable algorithms to compute the reverse euclidean distance transformation and discrete medial axis in arbitrary dimension. IEEE Transactions on Pattern Analysis and Machine Intelligence **29**(3), 437–448 (2007)
9. D. Attali, D.C., Remy, E.: Géométrie discrète et images numériques, chap. Représentation par axe médian, Chapitre 9. Trait IC2. Hermès (2007)
10. D. Attali, J.D.B., Edelsbrunner, H.: Stability and computation of medial axes: a state of the art report. In: Mathematical Foundations of Scientific Visualization, Computer Graphics, and Massive Data Exploration (2007)
11. Dey, T.K., Zhao, W.: Approximating the medial axis from the voronoi diagram with a convergence guarantee. Algorithmica **38**(1), 179–200 (2003)
12. E. C. Sherbrooke, N.M.P., Brisson, E.: Computation of the medial axis transform of 3-d polyhedra. In: SMA '95: Proceedings of the third ACM symposium on Solid modeling and applications, pp. 187–200 (1995)
13. F. Chazal, D.C.S., Lieutier, A.: A sampling theory for compact sets in euclidean space. In: SCG '06: Proceedings of the twenty-second annual symposium on Computational geometry, pp. 319–326 (2006)
14. F. Dellas, L. Moccozet, N. Magnenat-Thalmann, M. Mortara, G. Patane, M. Spagnuolo and B. Falcidieno: Knowledge-based extraction of control skeletons for animation. In: SMI '07: Proceedings of the IEEE International Conference on Shape Modeling and Applications 2007, pp. 51–60 (2007)
15. Ge, Y., Fitzpatrick, J.M.: On the generation of skeletons from discrete euclidean distance maps. IEEE Trans. Pattern Anal. Mach. Intell. **18**(11), 1055–1066 (1996)
16. Hulin, J., Thiel, E.: Chordal axis on weighted distance transforms. In: 13^{th} DGCI, Discrete Geometry for Computer Image, *Lectures Notes in Computer Science*, vol. 4245, pp. 271–282 (2006)
17. J. Jia, Z.Q., Lu, J.: Stratified helix information of medial-axis-points matching for 3d model retrieval. In: MIR '07: Proceedings of the international workshop on Workshop on multimedia information retrieval, pp. 169–176 (2007)
18. Kovalevsky, V.A.: Finite topology as applied to image analysis. Comput. Vision Graph. Image Process. **46**(2), 141–161 (1989)
19. N. Amenta, M.B., Kamvysselis, M.: A new voronoi-based surface reconstruction algorithm. In: SIGGRAPH '98: Proceedings of the 25th annual conference on Computer graphics and interactive techniques, pp. 415–421 (1998)
20. N. Amenta, S.C., Kolluri, R.: The power crust. In: Proceedings of 6th ACM Symposium on Solid Modeling, pp. 249–260 (2001)
21. P. Alliez D. Cohen-Steiner, M.Y., Desbrun, M.: Variational tetrahedral meshing. ACM Transactions on Graphics **24**(3), 617–625 (2005)
22. P. Alliez D. Cohen-Steiner, Y.T., Desbrun, M.: Voronoi-based variational reconstruction of unoriented point sets. In: SGP '07: Proceedings of the fifth Eurographics symposium on Geometry processing, pp. 39–48 (2007)
23. R. Fabbri L. F. Estrozi, L.D.F.C.: On voronoi diagrams and medial axes. J. Math. Imaging Vis. **17**(1), 27–40 (2002)
24. T. Ju, M.L.B., Chiu, W.: Computing a family of skeletons of volumetric models for shape description. Comput. Aided Des. **39**(5), 352–360 (2007)
25. Valette, S., Chassery, J.M., Prost, R.: Generic remeshing of 3d triangular meshes with metric-dependent discrete voronoi diagrams. IEEE Trans Visu Comp Graph pp. 369–381 (2007)
26. W. R. Quadros, K.S., Owen, S.J.: 3d discrete skeleton generation by wave propagation on pr-octree for finite element mesh sizing. In: SM '04: Proceedings of the ninth ACM symposium on Solid modeling and applications, pp. 327–332 (2004)